Removal of cationic dyes from aqueous solutions using $NiFe_2O_4$ nanoparticles

S. Sobhanardakani, R. Zandipak, H. Khoshsafar and R. Zandipak

ABSTRACT

In this study, $NiFe_2O_4$ nanoparticles ($NiFe_2O_4$ NPs) were synthesized and characterized by X-ray diffraction, transmission electronic microscopy (TEM), pH_{pzc} and Brunauer, Emmett, and Teller methods. The size of the nanostructures according to TEM was obtained and found to be around 12 nm. The adsorption capacity of $NiFe_2O_4$ NPs was examined using cationic dyes of malachite green (MG), Nile blue A (NB) and Janus green B (JG) as the pollutant (adsorbate). The results demonstrated that the optimum pH, adsorbent dose and temperature were 7.0, 0.05 g and 25 °C, respectively. Adsorption equilibrium experiments were performed, and the results of fitting by the non-linear models signify that the Langmuir–Freundlich model can describe the isotherm of adsorption. Also, the kinetic data were modeled with recently developed models, and the data indicate that the adsorption kinetics follow the fractal-like pseudo-second order ($r^2 > 0.99$). The method was applied to the removal of dyes in real samples. It was found that $NiFe_2O_4$ NPs is a highly efficient adsorbent for MG, NB and JG from aqueous solution, with a maximum capacity of 210 mg g^{-1}, 167.8 mg g^{-1} and 102.6 mg g^{-1}, respectively.

Key words | adsorption efficiency, isotherm, kinetic, $NiFe_2O_4$ nanoparticles

S. Sobhanardakani
Department of the Environment,
College of Basic Sciences,
Hamedan Branch,
Islamic Azad University,
Hamedan,
Iran

R. Zandipak (corresponding author)
H. Khoshsafar
Young Researchers & Elite Club,
Hamedan Branch,
Islamic Azad University,
Hamedan,
Iran
E-mail: *raziyeh.zandi@yahoo.com*

R. Zandipak
Department of Agriculture,
Payame Noor University,
Tehran,
Iran

INTRODUCTION

One of the most dangerous pollutants in water is synthetic dyes. They are used extensively in the textile, plastic, cosmetic, food and paper and other industries. These dyes are stable in light and heat, and resistant to oxidation and biodegradation (Wang *et al.* 2012). Hence, dyes can lead to acute effects on exposed organisms and aquatic life due to their toxicity, abnormal coloration and the reduction in photosynthesis (Chang *et al.* 2011; Satapanajaru *et al.* 2011). So the removal of dyes in water samples is important. Attention has been paid to physical (adsorption, membrane filtration, and ion exchange), chemical (oxidation, electrochemical degradation, and ozonation), and biological techniques for removal of dyes from wastewater, of which adsorption is efficient and economical (Li *et al.* 2012; Zhang *et al.* 2014).

A large number of adsorbents, such as porous carbon nanospheres/nanotubes, iron oxides, activated carbon, chitosan and core–shell nanoparticles, have been applied to remove dyes from wastewater (Gao *et al.* 2013; Ghaedi *et al.* 2014a; Kyzas *et al.* 2014).

In recent years, magnetic nanoparticles (NPs) with the general formula MFe_2O_4 (M = Fe, Co, Cu, Mn, Ni, etc.) are one of the most popular materials in analytical biochemistry, medicine, the removal of heavy metals and biotechnology, and have been increasingly applied to immobilize proteins, enzymes, and other bioactive agents due to their unique advantages (Sivakumar *et al.* 2012; Teymourian *et al.* 2013).

$NiFe_2O_4$ nanoparticles ($NiFe_2O_4$ NPs) are known as an adsorbent because of their good biocompatibility, strong super paramagnetic property, low toxicity, easy preparation and high adsorption ability (Khosravi & Eftekhar 2013). $NiFe_2O_4$ NPs with an inverse spinel structure shows ferrimagnetism that originates from the magnetic moment of anti-parallel spins between Fe^{3+} ions at tetrahedral sites and Ni^{2+} ions at octahedral sites. $NiFe_2O_4$ NPs exhibit high surface area and low mass transfer resistance. Moreover, the magnetic behavior of these nanoparticles depends mostly on their size (Patil *et al.* 2014).

doi: 10.2166/aqua.2015.046

In the present study, $NiFe_2O_4$ NPs were used for the removal of cationic dyes from aqueous solution. In batch tests, different parameters such as pH, contact time, amount of adsorbent and temperature were optimized for the adsorption process. Based on these studies, the isotherm and kinetics of adsorption were evaluated. Finally, the $NiFe_2O_4$ NPs were applied for the removal of dyes from water and food samples.

MATERIALS AND METHODS

Apparatus and reagents

All chemicals and reagents were purchased from Merck (Darmstadt, Germany). Stock solutions of dyes (10^{-3} mol L^{-1}) were prepared by dissolving the appropriate amount of their powder in double-distilled water (DDW). Dye solutions with initial concentrations of 40–500 mg L^{-1} were prepared by diluting the stock solution in appropriate proportions. Figure 1 shows the structure of the investigated dyes. DDW was used for all experiments.

The concentration of dye in the solutions was measured using a UV–Vis spectrophotometer (Lambda 45, Perkin-Elmer, USA). A pH meter (780, Metrohm, Switzerland) equipped with a combined Ag/AgCl glass electrode was used for pH measurements. The crystal structure of the synthesized materials was determined by X-ray diffraction (XRD) (ADP2000 ITALSTRUCTURE, Italy) at ambient temperature. The structure of the $NiFe_2O_4$ NPs was characterized by transmission electronic microscopy (TEM) (CM10, 100 KV, Philips). The elemental analysis was measured by scanning electron microscope energy dispersive X-ray spectroscopy (SEM-EDX) (XL30, Philips, The Netherlands). The specific surface area was defined by N_2 adsorption–desorption porosimetry (77 K) using a porosimeter (Bel, Japan).

Synthesis of $NiFe_2O_4$ NPs

The $NiFe_2O_4$ samples were prepared by the co-precipitation method. In a typical synthesis, a 0.2 M (20 mL) solution of iron nitrate [$(Fe(NO_3)_3.9H_2O)$] and a 0.1 M (20 mL) solution of nickel nitrate [$(Ni(NO_3)_2.6H_2O)$] were prepared and vigorously mixed under stirring for 1 h at 80 °C, and 0.2 g of polyethylene oxide was added into the solution as a capping agent. Subsequently, 5 mL of hydrazine hydrate ($NH_2{\cdot}NH_2{\cdot}H_2O$) was added drop by drop into the solution, and brown precipitates were formed. Finally, the precipitates were separated by centrifugation and dried in a hot air oven for 4 h at 100 °C. The acquired substance was annealed for 10 h at 300 °C.

Point of zero charge pH

The point of zero charge pH (pH_{pzc}) for the adsorbents was determined by introducing 0.05 g of $NiFe_2O_4$ NPs into eight 100 mL Erlenmeyer flasks containing 0.1 M $NaNO_3$ solution. The pH values of the solutions were adjusted to 2, 3, 4, 5, 6, 7, 8, and 9 using solutions of 0.01 mol L^{-1} HNO_3 and NaOH. The solution mixtures were allowed to equilibrate in an isothermal shaker (25 °C) for 24 h. The final pH was measured after 24 h. The pH_{pzc} is the point where the $pH_{initial} = pH_{final}$.

Adsorption experiment

Dye removal experiments with 0.05 g of $NiFe_2O_4$ NPs were performed in 25 mL stoppered conical flasks containing 10 mL of dye solution, at 40 mg L^{-1}. The pH of the solution was adjusted to 7.0 using 0.1 mol L^{-1} HCl and/or 0.1 mol L^{-1} NaOH solutions. The mixture was shaken at different time intervals (3–45 min) to facilitate adsorption of the dyes on the nanoparticles at 150 rpm at a temperature of 25 °C. Then dye loaded $NiFe_2O_4$ NPs were separated with magnetic

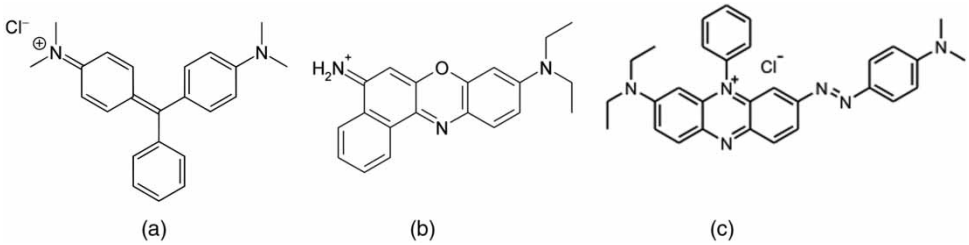

Figure 1 | Chemical structure of dye molecules: (a) MG, (b) NB and (c) JG.

decantation, and residual concentrations of malachite green (MG), Nile blue A (NB) and Janus green B (JG) were determined by UV–visible spectrophotometry (Lambda 45, Perkin-Elmer, USA) at 615, 635 nm, and 618 nm, respectively, and the amount of dyes adsorbed per unit mass of adsorbent at equilibrium conditions, q_e (mg g^{-1}), was evaluated based on Equation (1):

$$q_e = \frac{(C_0 - C_e)V}{W} \quad (1)$$

where C_0 and C_e are initial and equilibrium concentrations, respectively (mg L^{-1}), V (L) is the volume of solution and W (g) is the weight of adsorbent.

Finally, the removal efficiency for each dye was calculated using Equation (2):

$$R(\%) = \frac{C_0 - C_e}{C_0} \times 100 \quad (2)$$

where C_0 and C_e are the initial and final dye concentrations (mg L^{-1}).

Preparation of real samples

In order to demonstrate the applicability and reliability of the method for real samples, four samples, including tap water, river water, and jelly samples, were prepared and analyzed. Tap water samples were taken from our research laboratory (Islamic Azad University, Hamedan, Iran), river water was collected in a 2.0 L PTFE bottle. All water samples were filtered through a filter paper (Whatman No. 40) to remove suspended particulate matter.

Powdered jellies (blueberry and aloe vera) were purchased from a supermarket in Hamedan (Iran). The preparation instructions for the powdered jellies box specified 160 g L^{-1}. Solutions with 1.0 g L^{-1} of powdered jelly were prepared in water.

RESULTS AND DISCUSSION

Characterization of $NiFe_2O_4$

The XRD pattern of $NiFe_2O_4$ NPs is shown in Figure 2. Furthermore, it can be seen that all the diffraction peaks of

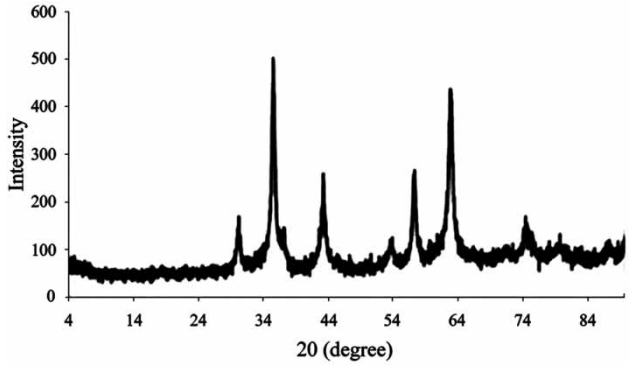

Figure 2 | The XRD pattern of $NiFe_2O_4$ NPs.

$NiFe_2O_4$ may be assigned to spinel type $NiFe_2O_4$ (JCPDS 54-0964). The peaks at the 2θ values of 30.1, 35.3, 43.0, 53.7, 56.5, and 62.4° can be indexed to (111), (220), (311), (400), (422), (511) and (440) crystal planes of spinel $NiFe_2O_4$, respectively. The average crystallite size (D in nm) of $NiFe_2O_4$ NPs was determined from the XRD pattern according to the Scherrer equation:

$$D = \frac{K\lambda}{\beta \cos\theta} \quad (3)$$

where λ is the wavelength of the X-ray radiation (1.5406Å), K is a constant taken as 0.89, θ is the diffraction angle and β is the full width at half maximum. The average size of the $NiFe_2O_4$ NPs was calculated as around 15 nm. The TEM micrograph and calculated histogram of the $NiFe_2O_4$, as shown in Figure 3, revealed that the diameter of the synthesized $NiFe_2O_4$ NPs was around 12 nm. The particle size measured directly from the TEM micrograph agrees with that determined by the XRD results. Figure 4 shows a typical SEM-EDX elemental analysis of $NiFe_2O_4$ NPs. The results demonstrate that only Ni, Fe and O appear in $NiFe_2O_4$ NPs samples.

Specific surface areas are commonly reported as Brunauer, Emmett, and Teller (BET) surface areas obtained by applying the theory of BET to nitrogen adsorption/desorption isotherms measured at 77 K. This is a standard procedure for the determination of the specific surface area of a sample. The specific surface area of the sample is determined by physical adsorption of a gas on the surface of the solid, and by measuring the amount of adsorbed gas corresponding to a monomolecular layer on the surface. The data are treated according to the BET theory (Brunauer *et al.* 1938). The results of the BET method showed that the average specific surface

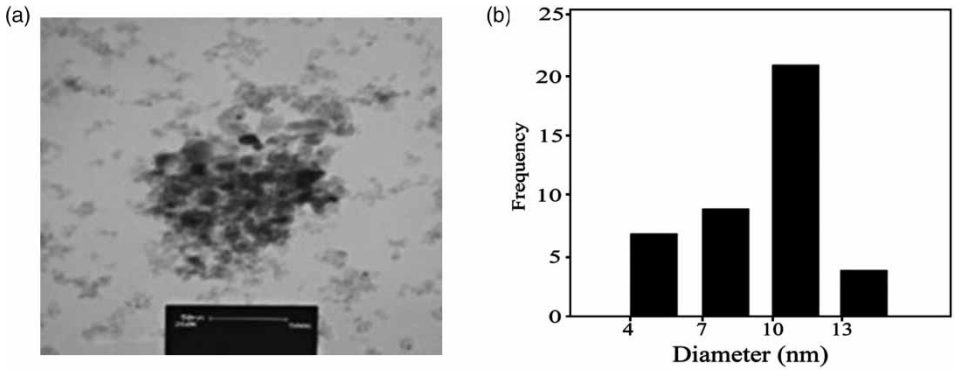

Figure 3 | (a) TEM micrograph and (b) calculated histogram of $NiFe_2O_4$ NPs.

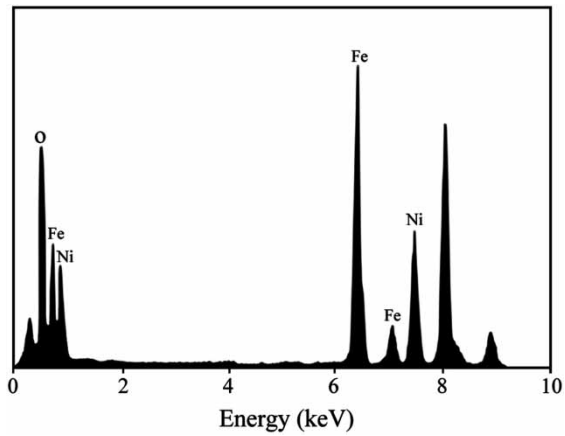

Figure 4 | SEM-EDX spectrum of $NiFe_2O_4$ NPs.

area of $NiFe_2O_4$ NPs was 63.7 $m^2 g^{-1}$. It can be concluded from these values that the synthesized nanoparticles have relatively large specific surface areas.

Effect of initial pH

The influence of pH of the aqueous solution is one of the main factors in the removal process. The effect of pH on the adsorption of MG, NB and JG onto $NiFe_2O_4$ NPs was studied at range of 2.0–9.0 for an initial dye concentration of 40 mg L^{-1}. It was observed from Figure 5(b) that the percentage of adsorption of dyes increased with an increase in the solution pH for all the three dyes studied. The maximum adsorption capacity of cationic dyes was observed at pH 7.0 and an increase in pH (>7.0) did not significantly change the dye removal capacity.

As observed in Figure 5(a), the point of zero charge for $NiFe_2O_4$ NPs is 7.0. The removal efficiencies of MG, NB and JG (cationic dyes) were low at pH < 7.0 (pH_{PZC} of $NiFe_2O_4$ NPs). The obvious decrease in removal might be attributed to the repulsive forces between the positive surface charge of $NiFe_2O_4$ NPs and the positive charge of the cationic dye. When the pH > 7.0, the removal of MG, NB and JG increased, this was put down to the attractive force of the negative surface charge of $NiFe_2O_4$ NPs and the positive charge of the dye. The decrease in the adsorption of dyes on $NiFe_2O_4$ NPs with a

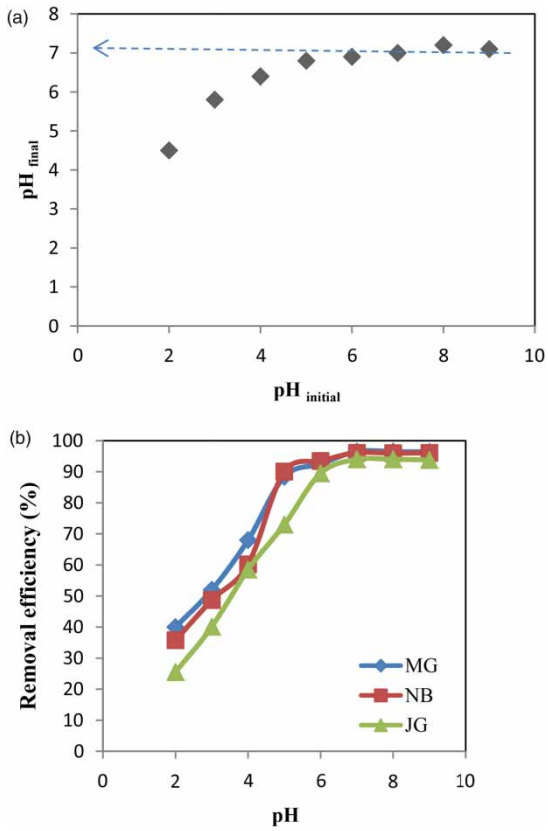

Figure 5 | (a) The determination of the point of zero charge of the $NiFe_2O_4$ NPs. (b) Effect of solution pH on the removal percentage of dyes by $NiFe_2O_4$ NPs.

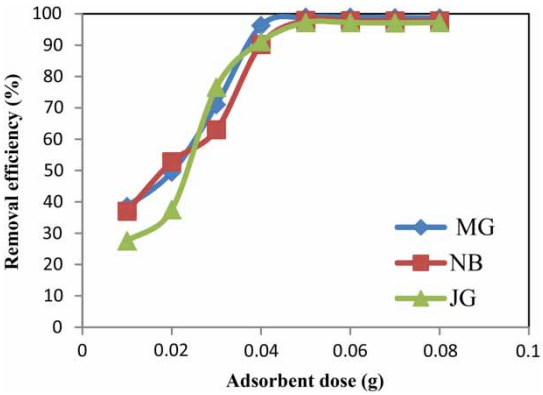

Figure 6 | Effect of dose of $NiFe_2O_4$ NPs on the removal percentage of dyes.

decrease in the solution pH might be attributed to competitive adsorption with the hydrogen ions at lower pH conditions.

Table 1 | Kinetic model equations

Kinetic model	Non-linear equation	Reference
PFO	$q_t = q_e(1 - \exp(-k_1 t))$	Azizian (2004)
PSO	$q_t = \frac{k_2 q_e^2 t}{1 + k_2 q_e t}$	Azizian (2004)
E	$q_t = \frac{1}{a} Ln(1 + abt)$	Piazinski *et al.* (2009)
EXP	$q_t = q_e Ln[2.72 - 1.72\exp(-k't)]$	Haerifar & Azizian (2013)
MOE	$q_t = q_e \frac{1 - \exp(-k_1 t)}{1 - F_2 \exp(-k_1 t)}$	Marczewski (2010)
FL-PSO	$q_t = \frac{k'_2 q_e^2 t^{\propto}}{1 + k'_2 q_e t^{\propto}}$	Haerifar & Azizian (2012)

Effect of adsorbent dose

Adsorbent dose is another important parameter because it determines the capacity of an adsorbent for a given initial concentration of adsorbate. The effect of the adsorption of dyes on the amount of $NiFe_2O_4$ NPs was studied at a temperature of 25 °C and at pH 7.0 by adding various amounts of adsorbent in the range of 0.01–0.08 g in contact with 40 mg L^{-1} of dyes. As shown in Figure 6, the adsorption of dyes increased with the increase in adsorbent dose, and reached a maximum level at a dose of 0.05 g. This observation can be explained by the increase in the surface area and availability of more active sites for adsorption. Therefore, 0.05 g of adsorbent was used in all experiments.

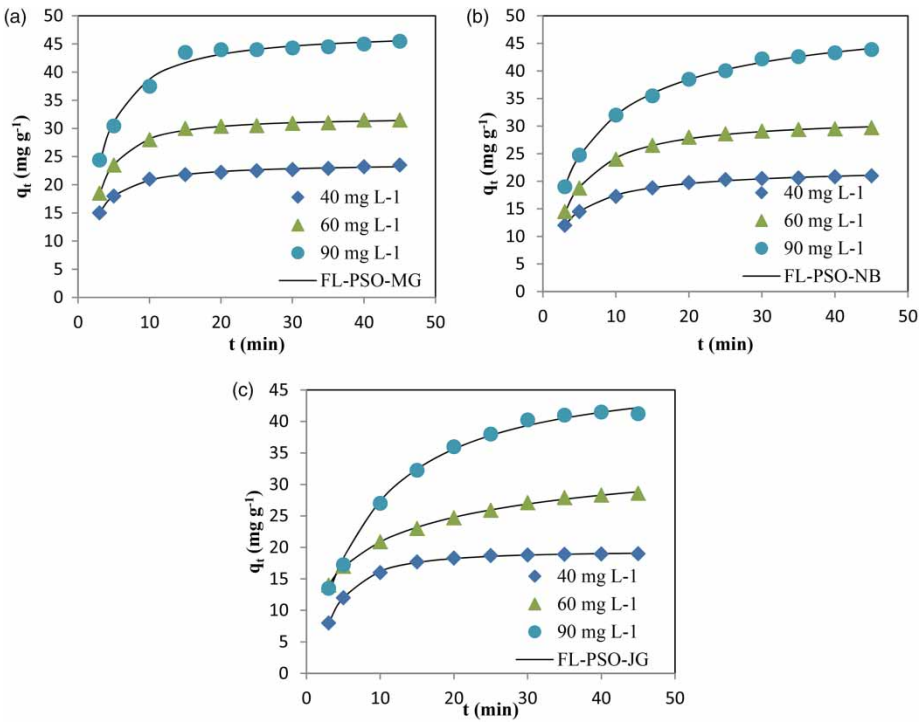

Figure 7 | Experimental kinetic data for the adsorption of (a) MG, (b) NB and (c) JG by $NiFe_2O_4$ NPs at different initial concentrations. Lines represent the FL-PSO model fitted to the data.

Table 2 | Constant of kinetic models for adsorption of dyes onto $NiFe_2O_4$ NPs

Kinetic model	dye	C_0 (mg L^{-1})	a	∝	k_2'	k_1'	b	F_2	k_1 (min^{-1})	k_2 (g mg^{-1} min)	q_e (mg g^{-1})	r^2	RMS error
PFO	MG	40	–	–	–	–	–	–	0.335	–	22.61	0.9534	0.620
		60	–	–	–	–	–	–	0.289	–	30.80	0.9820	0.607
		90	–	–	–	–	–	–	0.235	–	44.43	0.9733	1.26
PSO		40	–	–	–	–	–	–	–	0.023	24.23	0.9944	0.214
		60	–	–	–	–	–	–	–	0.013	33.38	0.9858	0.540
		90	–	–	–	–	–	–	–	0.006	49.05	0.9797	1.09
E		40	0.350	–	–	–	290.2	–	–	–	–	0.9220	0.802
		60	0.225	–	–	–	162.6	–	–	–	–	0.8934	1.48
		90	0.130	–	–	–	86.80	–	–	–	–	0.9085	2.33
EXP		40	–	–	–	0.246	–	–	–	–	22.70	0.9725	0.476
		60	–	–	–	0.211	–	–	–	–	30.96	0.9930	0.377
		90	–	–	–	0.169	–	–	–	–	44.77	0.9872	0.873
MOE		40	–	–	–	–	–	9.42	0.187	–	22.91	0.9847	0.379
		60	–	–	–	–	–	0.644	0.141	–	31.22	0.9965	0.285
		90	–	–	–	–	–	0.610	0.120	–	45.18	0.9855	0.987
FL-PSO		40	–	1.16	0.020	–	–	–	–	–	23.76	0.9965	0.179
		60	–	1.25	0.009	–	–	–	–	–	31.91	0.9981	0.209
		90	–	1.39	0.005	–	–	–	–	–	47.03	0.9897	0.846
PFO	NB	40	–	–	–	–	–	–	0.256	–	20.22	0.9336	0.837
		60	–	–	–	–	–	–	0.203	–	28.95	0.9772	0.837
		90	–	–	–	–	–	–	0.162	–	41.92	0.9507	2.003
PSO		40	–	–	–	–	–	–	–	0.017	22.22	0.9974	0.165
		60	–	–	–	–	–	–	–	0.008	32.51	0.9971	0.296
		90	–	–	–	–	–	–	–	0.004	48.34	0.9962	0.553
E		40	0.302	–	–	–	52.26	–	–	–	–	0.9635	0.620
		60	0.176	–	–	–	31.32	–	–	–	–	0.9496	1.24
		90	0.104	–	–	–	23.52	–	–	–	–	0.9887	0.957
EXP		40	–	–	–	0.182	–	–	–	–	20.39	0.9649	0.608
		60	–	–	–	0.144	–	–	–	–	29.27	0.9937	0.438
		90	–	–	–	0.112	–	–	–	–	42.67	0.9771	1.36
MOE		40	–	–	–	–	–	0.999	0.0001	–	22.30	0.9966	0.201
		60	–	–	–	–	–	1.37	0.075	–	41.36	0.9997	0.091
		90	–	–	–	–	–	0.999	0.0001	–	48.67	0.9956	0.635
FL-PSO		40	–	0.918	0.017	–	–	–	–	–	22.64	0.9980	0.152
		60	–	1.14	0.007	–	–	–	–	–	31.50	0.9989	0.189
		90	–	0.837	0.004	–	–	–	–	–	51.89	0.9988	0.326
PFO	JG	40	–	–	–	–	–	–	0.191	–	18.87	0.9978	0.183
		60	–	–	–	–	–	–	0.185	–	26.91	0.8940	1.73
		90	–	–	–	–	–	–	0.107	–	41.42	0.9930	0.904
PSO		40	–	–	–	–	–	–	–	0.011	21.37	0.9711	0.672
		60	–	–	–	–	–	–	–	0.007	30.58	0.9805	0.742
		90	–	–	–	–	–	–	–	0.107	41.42	0.9930	0.904
E		40	0.256	–	–	–	15.86	–	–	–	–	0.8926	1.297
		60	0.177	–	–	–	21.71	–	–	–	–	0.9977	0.253
		90	0.080	–	–	–	9.17	–	–	–	–	0.9771	1.64
EXP		40	–	–	–	0.136	–	–	–	–	19.08	0.9943	0.298
		60	–	–	–	0.127	–	–	–	–	27.35	0.9362	1.34
		90	–	–	–	0.072	–	–	–	–	42.73	0.9970	0.588

(*continued*)

Table 2 | continued

Kinetic model	dye	C_0 (mg L^{-1})	a	∝	k_2'	k_1'	b	F_2	k_1 (min^{-1})	k_2 (g mg^{-1} min)	q_e (mg g^{-1})	r^2	RMS error
MOE		40	–	–	–	–	–	0.061	0.183	–	18.89	0.9979	0.193
		60	–	–	–	–	–	0.999	0.0001	–	31.18	0.9747	0.907
		90	–	–	–	–	–	2.20	0.066	–	94.79	0.9968	0.654
FL-PSO		40	–	1.63	0.006	–	–	–	–	–	19.41	0.9994	0.103
		60	–	0.588	0.007	–	–	–	–	–	39.40	0.9990	0.178
		90	–	1.09	0.002	–	–	–	–	–	48.43	0.9951	0.810

Adsorption kinetic

Agitation time was one of the prime factors influencing the adsorption process. The influence of adsorption time on the adsorption capacity of the three dyes is shown in Figure 7. It can be seen that q_t increases rapidly during the initial adsorption stage, which was attributed to vacant surface sites available for adsorption. Subsequently, the diminishing availability of the remaining active sites and the decrease in the driving force led to the slow adsorptive process, and finally equilibrium was reached after approximately 10 min, 20 min and 15 min for MG, NB and JG, respectively, for an initial dye concentration of 40 mg L^{-1}. Also, the data presented in Figure 7 indicate the adsorption rate and the amount of dye adsorbed increases by increasing the initial dye concentration.

Table 3 | Obtained parameters for adsorption of dyes onto $NiFe_2O_4$ NPs

			Cationic dyes		
Isotherm	Non-linear equation	Parameters	MG	NB	JG
L	$q_e = \frac{q_m k_L C_e}{1 + k_L C_e}$	q_m(mg g^{-1})	199.1	161.9	106.2
		K_L(L mg^{-1})	0.104	0.025	0.027
		R_L	0.194	0.050	0.481
		r^2	0.9941	0.9970	0.9964
		RMS error	5.840	2.808	1.988
F	$q_e = k_f(C_e)^{1/n}$	K_F (L $mg^{(1-(1/n))}$/g)	45.99	17.77	14.32
		n	0.303	0.389	0.341
		r^2	0.9366	0.9619	0.9268
		RMS error	19.21	9.67	8.967
T	$q_e = Bln(AC_e)$	B	31.60	30.26	21.52
		A	3.089	0.413	0.314
		r^2	0.9724	0.9742	0.9861
		RMS error	12.66	7.948	3.902
B–S	$q_e = q_m(1 - \exp(-k_{B.S}C_e^a)$	q_m (mg g^{-1})	188.7	142.7	94.25
		A	0.685	0.792	0.833
		$K_{B\text{-}S}$(L $mg^{-1})^{\alpha}$	0.150	0.044	0.039
		r^2	0.9956	0.9972	0.9953
		RMS error	5.334	2.712	2.481
L–F	$q_e = \frac{q_m(kC_e)^{1/n}}{1 + (kC_e)^{1/n}}$	q_m(mg g^{-1})	210.0	167.8	102.6
		K_L(L mg^{-1})	0.091	0.023	0.029
		N	1.162	1.067	0.912
		r^2	0.9957	0.9973	0.9972
		RMS error	5.291	2.705	1.892
R–P	$q_e = \frac{k_{R-P}C_e}{1 + \propto' C_e^B}$	$K_{R\text{-}P}$ (L g^{-1})	23.69	4.150	2.687
		α' (L $mg^{-1})^{1/\beta}$	0.144	0.026	0.019
		B	0.960	0.994	1.04
		r^2	0.9948	0.9970	0.9969
		RMS error	6.020	2.965	1.994

The results showed that when the adsorbent was isolated immediately without a contact process into the samples, the analytes were hardly adsorbed. Agitation caused an increase in the adsorption and desorption rates.

Adsorption kinetics was investigated to describe the dye adsorption rate and eventually explore the mechanism of adsorption and possible rate-controlling steps. In order to analyze the adsorption kinetics of MG, NB and JG by adsorbent, the pseudo-first order (PFO), pseudo-second order (PSO), Elovich (E), mixed 1,2-order (MOE), exponential (EXP) and fractal-like pseudo-second order (FL-PSO) models (Table 1), were tested.

The results of fitting are listed in Table 2. According to the obtained correlation coefficients (r^2) for different initial concentrations of dyes, the experimental kinetic data were best fitted with the FL-PSO model. The following data obtained with the FL-PSO model indicate that the surface of the adsorbent is heterogeneous and the rate coefficient changes with time. It is also observed that the calculated equilibrium adsorption value (q_e) based on the FL-PSO model is close to the experimental equilibrium value. The result of fitting by FL-PSO is shown in Figure 7.

Adsorption isotherms and adsorption mechanism

An adsorption isotherm relates the relationship that exists between the amount of adsorbate adsorbed by the adsorbent (q_e) and the adsorbate concentration left in solution after equilibrium is attained (C_e) at a constant temperature. In the present study, the data obtained from the equilibrium adsorption experiments, at temperatures of 25 °C, were analyzed using the Langmuir (L) (Langmuir 1918), Freundlich (F) (Freundlich & Heller 1939), Temkin (T) (Temkin & Pyzhev 1940), Redlich–Peterson (R–P) (Mane *et al.* 2007), Langmuir–Freundlich (L–F) (Azizian *et al.* 2007) and Brouers–Sotolongo (B–S) (Brouers *et al.* 2005) models.

The parameters of fitting by the non-linear method are presented in Table 3. It was found that the L–F isotherm model shows high correlation coefficients ($r^2 > 0.99$) and a lower root mean square (RMS) error than other models. Another important criterion for evaluating the applicability of each model was based on the non-linear relative error (the best-fit isotherm). If the data from the model are similar to the experimental data, the RMS error will be a small number, if they are different, the RMS error will be a large

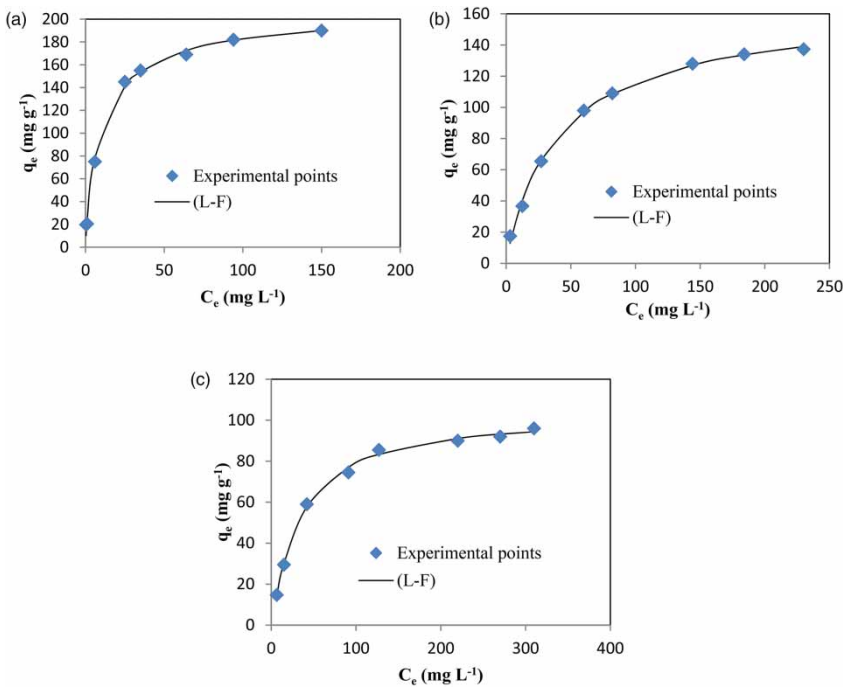

Figure 8 | Adsorption isotherms of (a) MG, (b) NB and (c) JG onto $NiFe_2O_4$ NPs. Lines represent the L–F model fitted to the data.

Table 4 | Comparison of maximum adsorption capacity (q_m) of different adsorbents for cationic dyes

	Maximum adsorption capacity (mg g^{-1})			
Adsorbent	**MG**	**NB**	**JG**	**Reference**
NiO flowerlike nanoarchitectures	142.08	–	–	Wei *et al.* (2014)
$Cd(OH)_2$-NW-AC	80.64	–	–	Ghaedi & Mosallanejad (2014b)
Oxide nanoparticle loaded on activated carbon	142.87	–	–	Shamsizadeh *et al.* (2014)
Natural clay	–	42	–	İyim & Güçlü (2009)
Oxidized multi-walled carbon nanotubes	–	–	56	Sobhanardakani *et al.* (2013)
Maghemite modified by SDS	–	–	172	Afkhami *et al.* (2010)
Mesoporous silica	–	–	61.82	Huang *et al.* (2011)
$NiFe_2O_4$ NPs	210	167.8	102.6	This work

number. Therefore, the good agreement between the adsorption data and the L–F model implies that the adsorption in all systems is heterogeneous. The results of fitting by this isotherm are shown in Figure 8. The adsorption capacities of MG, NB and JG on $NiFe_2O_4$ NPs were 210 mg g^{-1}, 167.8 mg g^{-1} and 102.6 mg g^{-1}, respectively. In Table 4, we compare the efficiency of the proposed adsorbent in the removal of cationic dyes from water with some other works. The results show that the $NiFe_2O_4$ NPs was efficient and had a much higher adsorption capability for cationic dyes.

Based on the results described, we propose that the mechanisms controlling the adsorption of MG, NB and JG on the $NiFe_2O_4$ NPs at solution pH 7.0 include: (i) electrostatic attraction between negatively charged $NiFe_2O_4$ NPs and positive dyes; and (ii) the cationic dyes can become adsorbed onto the $NiFe_2O_4$ NPs surface by coordination effect between metal ions and amine groups at the ends of dye molecules. At a low pH ($pH < pH_{PZC}$), the surface of the $NiFe_2O_4$ NPs is positively charged, which may produce repulsion to positive cationic dyes and the adsorption of dyes onto $NiFe_2O_4$ NPs is due to coordination between NH_2 on the surface of dyes and bivalence metal ions. At $pH > pH_{PZC}$, the synergistic effects of electrostatic attraction and coordination could be ascribed to the high adsorption of MG, NB and JG onto $NiFe_2O_4$ NPs.

Effect of temperature

The effect of temperature on the removal of cationic dyes was tested at four temperatures (25, 35, 45, 55 °C). The results of these experiments are presented in Figure 9, and show that the removal percentage of MG, NB and JG by $NiFe_2O_4$ NPs decreased with increasing temperature. Therefore, it is indicated that the adsorption of these dyes onto $NiFe_2O_4$ NPs is an exothermic process. The decrease in the rate of adsorption with the increase in temperature may be attributed to the weakening of the adsorptive forces between the active sites of the adsorbents and the adsorbate species.

Adsorption of cationic dyes in real samples

A standard addition method was applied to the adsorption of cationic dyes of MG, NB and JG in real samples such as water or industrial wastewater using $NiFe_2O_4$ NPs. The samples were also analyzed after spiking with different concentrations of dyes. The results are given in Table 5. The results show that the method is suitable for the analysis of real samples.

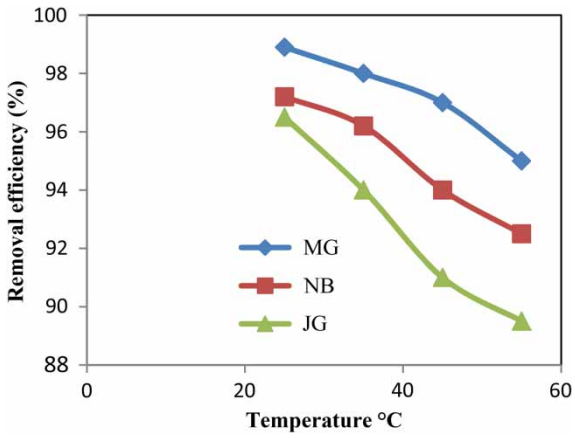

Figure 9 | Effect of temperature on the removal percentage of dyes by $NiFe_2O_4$ NPs.

Table 5 | Results of adsorption of cationic dyes in various real samples using $NiFe_2O_4$ NPs adsorbent under the optimum conditions ($n = 5$)

Sample	Dyes	Added ($\mu g\ L^{-1}$)	Found ($\mu g\ L^{-1}$)[a]	Recovery (%)
Tap water	MG	10	10.1 ± 0.04	101.0
		15	14.3 ± 0.32	95.3
	NB	10	9.9 ± 0.29	99.0
		15	14.8 ± 0.08	98.6
	JG	10	9.5 ± 0.15	95.0
		15	14.7 ± 0.58	98.0
River water	MG	10	9.8 ± 0.11	98.0
		15	15.4 ± 0.36	104.0
	NB	10	9.6 ± 0.05	96.0
		15	15.2 ± 0.15	102.0
	JG	10	10.3 ± 0.02	103.0
		15	15.1 ± 0.28	101.0
Blueberry powdered jelly	MG	25	26 ± 0.40	104.0
		50	51.3 ± 0.54	102.6
	NB	25	24.8 ± 0.23	99.2
		50	50.5 ± 0.47	101.0
	JG	25	25.2 ± 0.09	100.8
		50	48.7 ± 0.58	97.4
Aloe vera powdered jelly	MG	25	25.7 ± 0.13	102.8
		50	50.3 ± 0.31	100.6
	NB	25	24.1 ± 0.06	96.4
		50	49.5 ± 0.22	99.0
	JG	25	25.5 ± 0.19	102.0
		50	53.2 ± 0.54	106.4

[a]Mean of five determinations ± standard deviation.

Desorption studies

In order to evaluate the possibility of regeneration and reuse of the $NiFe_2O_4$ NPs adsorbent, desorption experiments have been performed. A desorption experiment was carried out with different eluents such as methanol, ethanol, acetic acid, NaOH and a mixture of methanol and sodium hydroxide. For this purpose, 10 mL of desorbent solution was added to the 0.05 g dye loaded $NiFe_2O_4$ NPs in a beaker. The nanoparticles were collected magnetically from the solution. The concentration of dyes in the desorbed solution was measured by UV–Vis spectrophotometery. The results are given in Figure 10. The results showed that the best eluent for the recovery of the $NiFe_2O_4$ NPs was a mixture of 0.1 mol L^{-1} NaOH and methanol. Then, the adsorbent was washed with DDW and reused for dye adsorption. The results showed that the reusability of the adsorbent was greater than four cycles without any loss in its adsorption behavior.

CONCLUSION

$NiFe_2O_4$ NPs are synthesized by the co-precipitation method and characterized by XRD analysis and TEM. The average particle size of $NiFe_2O_4$ is about 12 nm. The obtained $NiFe_2O_4$ NPs powders were tested for dye removal from aqueous solutions.

Maximum removal percentages have been obtained in neutral pH, and the variation of the dyes' uptake with the initial pH of the dye solution indicates that the main interaction between the dyes and the adsorbent is electrostatic attraction. The study of the effect of temperature on the adsorption of dyes by adsorbent indicated that the adsorption is an exothermic process. The equilibrium adsorption studies show that the equilibrium data follow the L–F isotherm, which indicates that the surface is heterogeneous. Also, the kinetics of dye adsorption onto the adsorbent follow the FL-PSO model, which indicate that the rate coefficient changes with time.

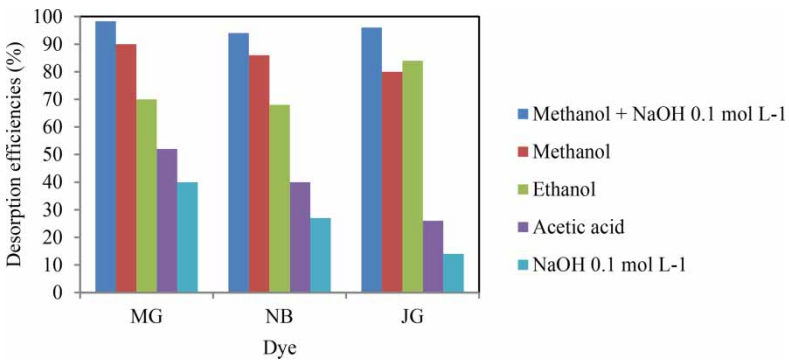

Figure 10 | Effect of type of eluting agent on recovery (%) for cationic dyes adsorbed on $NiFe_2O_4$.

REFERENCES

Afkhami, A., Saber-Tehrani, M. & Bagheri, H. 2010 Modified maghemite nanoparticles as an efficient adsorbent for removing some cationic dyes from aqueous solution. *Desalination* **263**, 240–248.

Azizian, S. 2004 Kinetic models of sorption: a theoretical analysis. *J. Colloid Interface Sci.* **276**, 47–52.

Azizian, S., Haerifar, M. & Basiri-Parsa, J. 2007 Extended geometric method: a simple approach to derive adsorption rate constants of Langmuir–Freundlich kinetics. *Chemosphere* **68**, 2040–2046.

Brouers, F., Sotolongo, O., Marquez, F. & Pirard, J. P. 2005 Microporous and heterogeneous surface adsorption isotherms arising from Levy distributions. *Phys. A* **349**, 271–282.

Brunauer, S., Emmett, P. H. & Teller, E. 1938 Adsorption of gases in multimolecular layers. *J. Am. Chem. Soc.* **60**, 309–319.

Chang, Y. P., Ren, C. L., Yang, Q., Zhang, Z. Y., Dong, L. J., Chen, X. G. & Xuec, D. S. 2011 Preparation and characterization of hexadecyl functionalized magnetic silica nanoparticles and its application in Rhodamine 6G removal. *Appl. Surf. Sci.* **257**, 8610–8616.

Freundlich, H. & Heller, W. 1939 The adsorption of cis- and trans-Azobenzene. *J. Am. Chem. Soc.* **61**, 2228–2230.

Gao, H., Zhao, S., Cheng, X., Wang, X. & Zheng, L. 2013 Removal of anionic azo dyes from aqueous solution using magnetic polymer multi-wall carbon nanotube nanocomposite as adsorbent. *Chem. Eng. J.* **223**, 84–90.

Ghaedi, M., Negintaji, G., Karimi, H. & Marahel, F. 2014a Solid phase extraction and removal of brilliant green dye on zinc oxide nanoparticles loaded on activated carbon: new kinetic model and thermodynamic evaluation. *J. Ind. Eng. Chem.* **20**, 1444–1452.

Ghaedi, M. & Mosallanejad, N. 2014b Study of competitive adsorption of malachite green and sunset yellow dyes on cadmium hydroxide nanowires loaded on activated carbon. *J. Ind. Eng. Chem.* **20**, 1085–1096.

Haerifar, M. & Azizian, S. 2012 Fractal-like adsorption kinetics at the solid/solution Interface. *J. Phys. Chem. C* **116**, 13111–13119.

Haerifar, M. & Azizian, S. 2013 An exponential kinetic model for adsorption at solid/solution interface. *Chem. Eng. J.* **215–216**, 65–71.

Huang, C. H., Chang, K. P., Ou, H. D., Chiang, Y. C. & Wang, C. F. 2011 Adsorption of cationic dyes onto mesoporous silica. *Micropor. Mesopor. Mater.* **141**, 102–109.

İyim, T. B. & Güçlü, G. 2009 Removal of basic dyes from aqueous solutions using natural clay. *Desalination* **249**, 1377–1379.

Khosravi, I. & Eftekhar, M. 2013 Characterization and evaluation catalytic efficiency of $NiFe_2O_4$ nanospinel in removal of reactive dye from aqueous solution. *Powder Technol.* **250**, 147–153.

Kyzas, G. Z., Lazaridis, N. K. & Kostoglou, M. 2014 Adsorption/desorption of a dye by a chitosan derivative: experiments and phenomenological modeling. *Chem. Eng. J.* **248**, 327–336.

Langmuir, I. 1918 The adsorption of gases on plane surfaces of glass, mica and platinum. *J. Am. Chem. Soc.* **40**, 1361–1403.

Li, X., Xiao, W., He, G., Zheng, W., Yu, N. & Tan, M. 2012 Pore size and surface area control of MgO nanostructures using a surfactant-templated hydrothermal process: high adsorption capability to azo dyes. *Colloid. Surf. A* **408**, 79–86.

Mane, V. S., Mall, I. D. & Srivastava, V. C. 2007 Kinetic and equilibrium isotherm studies for the adsorptive removal of Brilliant Green dye from aqueous solution by rice husk ash. *J. Environ. Manage.* **84**, 390–400.

Marczewski, A. W. 2010 Application of mixed order rate equations to adsorption of methylene blue on mesoporous carbons. *Appl. Surf. Sci.* **256**, 5145–5152.

Patil, J. Y., Nadargi, D. Y., Gurav, J. L., Mulla, I. S. & Suryavanshi, S. S. 2014 Synthesis of glycinecombusted $NiFe_2O_4$ spinel ferrite: a highly versatile gas sensor. *Mater. Lett.* **124**, 144–147.

Piazinski, W., Rudzinski, W. & Plazinska, A. 2009 Theoretical models of sorption kinetics including a surface reaction mechanism: a review. *J. Colloid Interface Sci.* **152**, 2–13.

Satapanajaru, T., Chompuchan, C., Suntornchot, P. & Pengthamkeerati, P. 2011 Enhancing decolorization of Reactive Black 5 and Reactive Red 198 during nano zero valent iron treatment. *Desalination* **266**, 218–230.

Shamsizadeh, A., Ghaedi, M., Ansari, A., Azizian, S. & Purkait, M. K. 2014 Tin oxide nanoparticle loaded on activated carbon as new adsorbent for efficient removal of malachite green-oxalate: non-linear kinetics and isotherm study. *J. Mol. Liquids* **195**, 212–218.

Sivakumar, P., Ramesh, R., Ramanand, A., Ponnusamy, S. & Muthamizhchelvan, C. 2012 Synthesis, studies and growth mechanism of ferromagnetic $NiFe_2O_4$ nanosheet. *Appl. Surf. Sci.* **258**, 6648–6652.

Sobhanardakani, S., Zandipak, R. & Sahraei, R. 2013 Removal of Janus Green dye from aqueous solutions using oxidized multi-walled carbon nanotubes. *Toxicol. Environ. Chem.* **95** (6), 909–918.

Temkin, M. J. & Pyzhev, V. 1940 Recent modifications to Langmuir isotherms. *Acta Physio. Chim.* **12**, 217–222.

Teymourian, H., Salimi, A. & Khezrian, S. 2013 Fe_3O_4 magnetic nanoparticles/reduced graphene oxide nanosheets as a novel electrochemical and bioeletrochemical sensing platform. *Biosens. Bioelectron.* **49**, 1–8.

Wang, Y. F., Gao, B. Y., Yue, Q. Y., Wang, Y. & Yang, Z. L. 2012 Removal of acid and direct dye by epichlorohydrin–dimethylamine: flocculation performance and floc aggregation properties. *Bioresour. Technol.* **113**, 265–271.

Wei, A., Liu, B., Zhao, H., Chen, Y., Wang, W., Ma, Y., Yang, H. & Liu, S. 2014 Synthesis and formation mechanism of flowerlike architectures assembled from ultrathin NiO nanoflakes and their adsorption to malachite green and acid red in water. *Chem. Eng. J.* **239**, 141–148.

Zhang, Y. R., Shen, S. L., Wang, S. Q., Huang, J., Su, P., Wang, Q. R. & Zhao, B. X. 2014 A dual function magnetic nanomaterial modified with lysine for removal of organic dyes from water solution. *Chem. Eng. J.* **239**, 250–256.

First received 5 April 2015; accepted in revised form 4 September 2015. Available online 19 October 2015